The Reaction of CH_2 (X^3B_1) with O_2 ($X^3\Sigma_g^-$): A Theoretical CASSCF/CASPT2 Investigation

B.-Z. Chen,[†] J. M. Anglada,*[,‡] M.-B. Huang,*[,†] and F. Kong[§]

Graduate School, Academia Sinica, P.O. Box 3908, Beijing 100039, P. R. China, Department de Química Orgànica Biológica, Institut d'Investigacions Químiques i Ambientals de Barcelona, CSIC, C/ Jordi Girona 18, E-08034 Barcelona, Spain, and Institute of Chemistry, Academia Sinica, Beijing 100080, P. R. China

Received: November 26, 2001; In Final Form: January 7, 2002

The reaction between CH_2 (X^3B_1) + O_2 in the gas phase was investigated by carrying out CASSCF and CASPT2 calculations with the 6-31G(d,p) and 6-311+G(3df,2p) basis sets. The reaction proceeds by the addition of O_2 to methylene and may follow a singlet and a triplet potential energy surface. In both cases, its fate is the carbonyl oxide (H_2COO). The reaction in its singlet multiplicity is computed to be exothermic by 50.9 kcal/mol with an activation enthalpy of 1.9 kcal/mol at 298 K. The reaction in its triplet multiplicity is computed to be exothermic by 26.9 kcal/mol with an activation enthalpy of 5.4 kcal/mol at 298 K. According to classical transition state theory, the branching ratio for the reaction in its triplet state multiplicity changes from negligible at 298 K to about 26% at 1800 K, and this ratio equals the formation of atomic oxygen (O, ^3P). The following unimolecular decomposition of carbonyl oxides in its singlet and triplet multiplicity was also considered.

Introduction

The reaction of methylene (CH_2) with O_2 is one of the most important reactions in the combustion of unsaturated hydrocarbons[1−3] and has been investigated by several experimental techniques.[1−9] Bley et al. and Dombrowsky et al.[4−6] observed OH radical and H and O atoms by atomic resonance absorption spectroscopy and ESR, while as stable products, CO, CO_2, H_2CO, HCOOH, and H_2O were reported.[3,9−12] Estimates of the rate constant measured in the 295−1800 K range have been also reported in the literature,[3,6,14−17] and the recommended values at $T = 298$ K are in the $(1.2-1.7) \times 10^{-12}$ cm^3 molecule^{-1} s^{-1} range. In addition, photolysis of CH_2CO in the presence of O_2 produces $H_2CO + O_3$. Here, the ketene photolysis produces CH_2, and the formation of $H_2CO + O$ (^3P) was suggested as a first-step reaction between CH_2 (X^3B_1) and O_2, preceding the formation of O_3 by reaction between O_2 and O (^3P).[13]

Regarding the reaction mechanism, Dombrowsky et al.[5] and Su et al.[9] suggested that the first step of the $CH_2 + O_2$ reaction could be the formation of the carbonyl oxide (H_2COO) intermediate, which can rearrange to dioxirane and methylenebis(oxy) isomers before dissociation. However, as far as we know, there is not a theoretical study concerning the detailed mechanism of the reaction between CH_2 and O_2. On the other side, the intermediate carbonyl oxide and its isomerization and dissociation processes have received a great amount of interest in the past few years, both experimentally[18−24] and theoretically,[25−35] because of its importance in atmospheric chemistry as a result of the alkene ozonolysis. In fact, the stable compounds CO, CO_2, H_2CO, HCOOH, and H_2O are observed as a fate of the unimolecular decomposition of carbonyl oxide.[18−20]

The aim of the present study is to perform a theoretical investigation on the reaction between CH_2 (X^3B_1) and O_2 ($X^3\Sigma_g^-$). This reaction can proceed via singlet, triplet, and quintet potential energy surfaces (PESs). The quintet state requires a parallel alignment of the four electrons of both triplet reactants, and therefore, the corresponding PES is expected to have repulsive character and was not considered. However, the triplet and singlet PESs are expected to have bonding character and have been investigated in the present work. Both reaction channels proceed via the carbonyl oxide (H_2COO) intermediates in these singlet and triplet electronic states, and therefore, we have also considered the processes that lead to their unimolecular decomposition.

Computational Methods

The geometries of all stationary points were located by the use of CASSCF wave functions[36] with analytical gradient procedures.[37−39] The character of each stationary point (minima or saddle point) was checked by performing frequency analysis calculations, which are also used to derive the corresponding zero-point energies (ZPE) and the corresponding enthalpy and entropy corrections. The ZPEs were scaled by 0.8929 to take into account the anharmonic effects.[40] Furthermore, to ensure that each transition structure connects a reactant with a product in every elementary reaction, we have carried out intrinsic reaction coordinate (IRC) calculation starting at the corresponding transition state. The active spaces of the CASSCF wave functions were selected according to the fractional occupation of a set of natural orbitals (NOs)[41] generated from a multireference single and double configuration interaction (MRD-CI) wave function[42−44] correlating all valence electrons. The active space composition of all stationary points considered is schematized in Table 1 of the Supporting Information.

In a first step, all geometry optimizations were performed using the 6-31G(d,p) basis set.[45] However, for the reactants (CH_2 and O_2), the carbonyl oxides, and the corresponding transition

* To whom correspondence should be addressed. E-mail for J.M.A.: anglada@iiqab.csic.es.
[†] Graduate School, Academia Sinica.
[‡] Institut d'Investigacions Químiques i Ambientals de Barcelona.
[§] Institute of Chemistry, Academia Sinica.

10.1021/jp014319x CCC: $22.00
Published on Web 02/02/2002

structures, in both the singlet and triplet states, CASSCF geometry reoptimizations were also carried out by using the larger 6-311+G(3df,2p) basis set.[46] In these cases, the frequency analysis was also done employing the larger basis set. In some other selected cases also, geometry optimizations were carried out employing this larger 6-311+G(3df,2p) basis set.

The effect of the dynamic valence electron correlation on the relative energy of the CASSCF stationary points was incorporated by carrying out single-point CASPT2 calculations[47,48] and using the larger 6-311+G(3df,2p) basis set. In this case, the CASPT2 calculations were based on a common CASSCF(18,14) wave function, which leads to more than 4×10^6 determinants in C_1 symmetry. In this active space, only the 1s electrons of the carbon and the two oxygen atoms are considered as a core while the virtual orbitals were also selected according to the occupation of the NOs derived from a single-point MRD-CI calculation. The results presented in this work were obtained employing the Gaussian 98,[49] GAMESS,[50] Molcas 4.1,[51] and MRD-CI program packages.

For the $CH_2 + O_2$ elementary reactions, we have also computed the rate constants using classical transition-state theory. These rate constants were calculated employing the CASPT2/6-311+G(3df,2p) energies and the partition functions and zero-point corrections energies obtained at the CASSCF/6-311+G(3df,2p) level. The tunneling corrections to the rate constant were also considered and computed by the zero-order approximation to the vibrationally adiabatic PES with zero curvature,[52] where an unsymmetrical Eckart potential energy barrier approximates the potential energy curve. The Rate program by Truong et al.[53] was used for this purpose.

Results and Discussion

We have designated the structures of the stationary points by **im** for the minima and **imts** for the transition states, followed by a number (**1**, **2**, and so on). To distinguish the structures of the singlet and triplet PESs, we have appended the letter **T** to indicate that the corresponding structure has triplet multiplicity. Otherwise, it is assumed that the corresponding structure possesses singlet multiplicity. In Table 1, we have collected for each structure the zero-point energy (ZPE), entropy (*S*), and the relative energies and the ZPE-corrected relative energies of all elementary reactions considered, which were obtained with the best theoretical treatment in each case. The enthalpies and free energies computed at 298 K are also included to allow comparison of the data with other results from the literature. Figures 1 and 3 collect the most relevant geometrical parameters of each optimized stationary structure, while Figure 2 displays a schematic potential enthalpy profile of the whole process considered**.** Table 3 displays the calculated rate constants for the $CH_2 + O_2$ reaction as well as the computed branching ratio for the triplet PES, while Table 4 contains the harmonic vibrational frequencies and IR intensities for **im1**, **im2**, and **im1T**. The Cartesian coordinates and absolute energies of all structures reported in this paper are available as a Supporting Information or from the authors upon request.

The Reaction between CH_2 (X^3B_1) and O_2 ($X^3\Sigma_g^-$). The first stage of the reaction corresponds to the addition of molecular oxygen to CH_2, which can proceed via singlet and triplet electronic states. In each case, the fate of the reaction is the intermediate carbonyl oxide (H_2COO) in its singlet and triplet multiplicities, respectively.

Regarding the singlet PES, Figure 1 shows that the formation of carbonyl oxide **im1** (C_S , X^1A') occurs through the symmetric transition state **imts1** (C_S, $^1A'$). The attack of the molecular

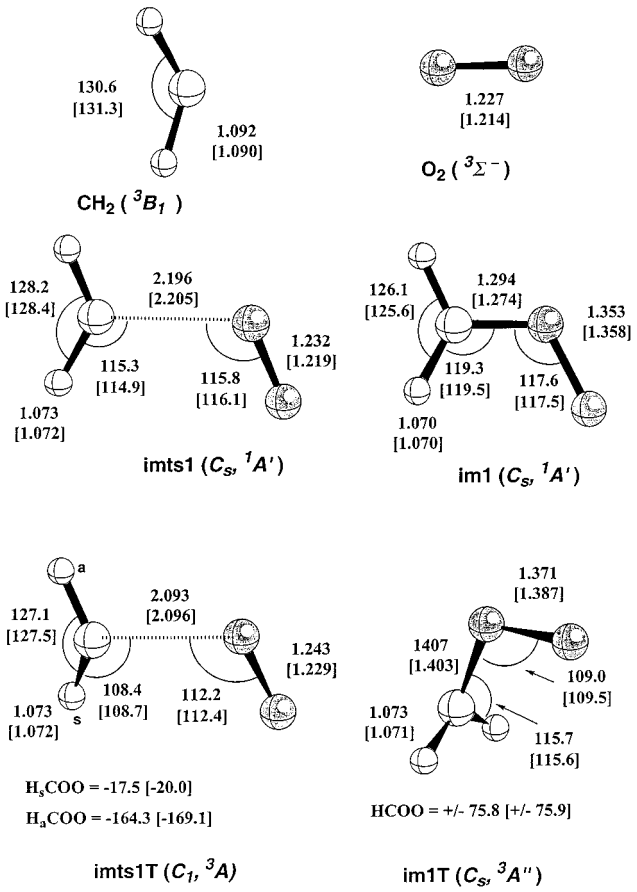

Figure 1. Selected geometrical parameters of the CASSCF/6-31G-(d,p) and CASSCF/6-311+G(3df,2p), in square brackets, for the stationary points involved in the reaction between CH_2 and O_2.

oxygen to CH_2 is of the end-on type, and all five atoms lie in the same plane as in the reaction product **im1**. Thus, the reaction takes place entirely in the C_S plane. The analysis of the geometrical parameters displayed in Figure 1 shows a large CO bond distance (2.205 Å) and a small OO bond length (1.219 Å), which suggest an early transition state. Moreover, comparing the results obtained using both basis sets, we observe quite similar geometrical parameters, the larger difference being the CO bond length in **im1**, which is 0.02 Å smaller in the best treatment. For **im1**, the geometrical parameters compare also with previous results from the literature,[29,31,32,35] although the OO bond distance is 0.024 Å larger than the most accurate results reported at the CCSD(T) level with a large basis set.[35]

In the triplet PES, the oxygen attack to CH_2 is also of an end-on fashion. Figure 1 shows that the corresponding transition structure (**imts1T**) is not symmetric anymore but deviates slightly, about 20°, from the plane. The CO bond length is computed to be 2.096 Å, which is about 0.1 Å shorter than the corresponding one in the singlet PES. The C atom is slightly pyramidalized as one of the unpaired electrons is going to be mainly located on it in the final product (triplet H_2COO, **im1T**), Please note that **im1T** has C_s symmetry ($^3A''$) and that the OOC and HCH planes are perpendicular to each other as discussed previously in the literature. [32] The geometrical parameters obtained in both basis sets are also quite similar and for **im1T** compare very well with previously reported values.[32]

In addition, we have also looked for other possible reaction modes in both the triplet and singlet PESs. In particular, we have found saddle-point structures (for the singlet and triplet PESs), which correspond to a side-on attack of O_2 to CH_2. However, these saddle points possess two imaginary frequencies.

TABLE 1: Zero-Point Energy Corrections (ZPE in kcal/mol), Entropy (*S* in eu) and the Best Values Corresponding to the Relative Energies, Energies Including the ZPE Corrections, Enthalpies, and Free Energies (in kcal/mol) for the Singlet and Triple PES

compound	ZPE[a]	*S*	relative to	ΔE	$\Delta(E + \text{ZPE})$	ΔH	ΔG
			Singlet PES				
imts1	13.4	67.6	$CH_2 + O_2$	0.5	2.4	1.9	10.3
im1	17.7	59.7	**imts1**	−56.7	−52.3	−52.8	−50.5
imts2	16.7	59.6	**im1**	20.1	19.0	18.9	18.9
im2	19.1	57.5	**imts2**	−48.7	−46.3	−46.1	−48.7
imts3	15.4	59.4	**im1**	35.2	32.9	32.5	32.6
im3	17.4	60.5	**imts3**	−26.7	−24.7	−24.2	−24.6
imts4	17.3	59.3	**im2**	20.6	18.8	18.5	18.0
im4	17.3	58.6	**imts4**	−15.2	−15.1	−14.9	−14.7
imts5	15.7	59.5	**im4**	3.8	2.2	1.9	1.6
im5b	19.9	59.2	**imts5**	−98.0	−93.9	−93.4	−93.3
imts6	15.0	58.2	**im4**	0.6	−1.7	−1.9	−1.8
imts7	15.6	62.1	**im5b**	69.8	65.5	65.4	64.6
im5a	19.6	59.5	**im5b**	4.7	4.4	4.5	4.4
imts8	14.1	59.2	**im5a**	68.3	62.8	62.1	62.2
imts10	18.7	58.9	**im5b**	11.1	9.9	9.7	9.8
$CO_2 + H_2$	11.0	83.6	**imts8**	−82.7	−85.7	−84.4	−91.7
$CO + H_2O$	14.8	92.4	**imts7**	−61.7	−62.4	−61.0	−70.1
Imts9	13.5	59.9	**im4**	24.9	21.1	20.6	20.2
HCOO + H	11.8	87.5	**imts9**	−5.0	−6.7	−5.5	−13.7
$CO_2 + 2H$	5.4	107.2	HCOO + H	−16.4	−22.8	−22.3	−28.2
			Triplet PES				
imts1T	13.6	69.0	$CH_2 + O_2$	4.0	6.1	5.4	13.1
im1T	16.3	66.2	**imts1T**	−34.9	−32.2	−32.3	−31.4
imts2T	15.4	64.9	**im1T**	4.1	3.2	2.9	3.4
$H_2CO + O(^3P)$	15.7	53.6	**imts2T**	−31.8	−31.5	−32.0	−28.8

[a] The ZPE values are scaled by 0.8929 to consider the anharmonic effects.

The analysis of the vector corresponding to the second imaginary frequency indicated a movement toward the end-on-type attack as described above, and therefore, we concluded that **imts1** and **imts1T** are the unique reaction modes for this reaction. Furthermore, we have also looked for the possible existence of van der Waals complexes between CH_2 and O_2, but no such like complexes were found in the present investigation. Because we have used a CASSCF approach, which does not include dynamical correlation energy, we cannot definitely exclude the possible existence of such van der Waals complexes. Because of the multiconfigurational character of the wave function (see below), a proper treatment of these structures would require a multireference method as CASPT2. However, the Molcas 4.1 has not gradients available at CASPT2 level, and a point-wise search using a CASSCF(18,14) reference function is beyond our computer facilities.

From an energetic point of view, our best calculations from Table 1 show that reactions are computed to be exothermic by 56.2 kcal/mol ($\Delta H = -50.9$ kcal/mol) and 30.9 kcal/mol ($\Delta H = -26.9$ kcal/mol) for the singlet (**im1**) and the triplet (**im1T**) PES, respectively, the singlet **im1** being 25.3 kcal/mol more stable than the triplet **im1T** (24 kcal/mol considering the enthalpy corrections), which compares with the 24.1 kcal/mol value reported in the literature.[32] The corresponding energy barriers are computed to be 0.5 kcal/mol ($\Delta H = 1.9$ kcal/mol) for **imts1** and 4.0 kcal/mol ($\Delta H = 5.4$ kcal/mol) for **imts1T**, respectively. It is here remarkable that the energy barrier for the singlet PES is considerably lower than that of the triplet PES. This fact can be rationalized by looking at the electronic structure of the corresponding CASSCF wave functions, which are displayed in Table 2. The triplet transition state **imts1T** is mainly characterized by two electronic configurations, which differentiate from each other by the double excitation $11a^2 \rightarrow 14a^2$. The natural orbital occupation of the CASSCF wave function, 1.62 for the 11a orbital (σ(CO) character) and 0.41 for the 14a orbital (σ^*(CO) character), points out the formation of the CO bond, while the unpaired electrons are already located on the C and the terminal O, respectively, as in the product **im1T** (C_S, ^{3}A") (see Figure 1 and ref 32). On the other side, Table 2 shows that the transition structure for the singlet PES (**imts1**) possesses a very complex electronic description, with five electronic configurations having a very important weight. This fact makes clear the need to use theoretical approaches that can take into account the multiconfigurational character of the wave function to obtain a correct description of this process. It is interesting to note the natural occupation of the 10a' and 11a' orbitals (1.52 and 0.52), which possess σ(CO) and σ^*(CO) character, respectively, and that of the 2a" and 3a" orbitals (1.23 and 0.81), corresponding to the π(CO) and π^*(CO), respectively. This fact reflects clearly the simultaneous formation of the σ and π bonds in the singlet PES, which produces an extra stabilization of this transition structure with respect to the triplet transition state.

TABLE 2: Character of the CASSCF Wave Function Corresponding to imts1 and imts1T Transition States

imts1 (C_s, ^{1}A')

coeff[a]	8a'	9a'	10a'	1a"	2a"	11a'	12a'	3a"
0.63	2	2	2	2	2	0	0	0
−0.47	2	2	2	2	0	0	0	2
0.33	2	2	1	2	1	1	0	1
−0.30	2	2	0	2	2	2	0	0
0.27	2	2	0	2	0	2	0	2
occ[a]	1.96	1.96	1.52	1.96	1.23	0.52	0.04	0.81

imts1T (C_1, ^{3}A)

coeff[a]	8a	9a	10a	11a	12a	13a	14a	15a
0.84	2	2	2	2	1	1	0	0
−0.35	2	2	2	0	1	1	2	0
occ[a]	1.96	1.96	1.96	1.62	1.05	0.99	0.41	0.05

[a] The abbreviations coeff and occ stand for the coefficient of the leading configuration and the natural orbital occupation of the CASSCF wave function, respectively.

Finally, to determine the competition between the singlet and the triplet PESs, we have computed rate constants in the 250−1800 K range, utilizing classical transition-state theory. The corresponding values, K_s for the singlet and K_t for the triplet, are displayed in Table 3, which also contains the computed branching ratio, Γ, corresponding to the triplet PES. Here, Γ is simply calculated as K_t/K where K is the sum of rate constants $K_s + K_t$. Table 3 shows important discrepancies for the computed rate constant at $T = 298$ K. Our calculated rate constant is about 300 times smaller than the estimated experimental values (in the $(1.2-1.7) \times 10^{-12}$ cm^3 molecule^{-1} s^{-1} range at $T = 298$ K).[14−16] Despite this difference, this should not have a strong effect in the calculation of the branching ratio of the triplet PES because both the single and the triplet paths are computed at the same level of theory and the corresponding activation energies are expected to suffer the same error. Because **im1T** dissociates into $H_2CO + O(^3P)$, [32] the branching ration of the triplet PES is equivalent to the O atom production in its ground state (^{3}P). The computed values displayed in Table 3 indicate that Γ(O) is very low or negligible at low T but rises up to about 26% at 1800 K. These values may be compared with an estimated mean channel distribution of O (^{3}P) of about 10% reported in the 1000−1800 K range.[5,6]

Unimolecular Decomposition of the Singlet Carbonyl Oxide (H_2COO, X^1A'). The unimolecular decomposition of carbonyl oxide has received much interest in the past few years because of its importance in tropospheric chemistry because it

TABLE 3: Calculated Rate Constants (in cm^3 molecule^{-1} s^{-1}) at Different Temperatures (T in K) for the CH_2 (X^3B_1) + O_2 ($X^3\Sigma^-$) Reaction[a]

T	K_s	K_t	$K_s + K_t$	Γ
250	3.317×10^{-15}	1.422×10^{-18}	3.318×10^{-15}	0.04
298	6.453×10^{-15}	1.130×10^{-17}	6.464×10^{-15}	0.17
350	1.151×10^{-14}	5.901×10^{-17}	1.157×10^{-14}	0.51
400	1.982×10^{-14}	2.003×10^{-16}	2.002×10^{-14}	1.00
450	3.172×10^{-14}	5.341×10^{-16}	3.225×10^{-14}	1.66
500	4.735×10^{-14}	1.199×10^{-15}	4.854×10^{-14}	2.47
600	9.119×10^{-14}	4.263×10^{-15}	9.545×10^{-14}	4.47
700	1.538×10^{-13}	1.114×10^{-14}	1.650×10^{-13}	6.75
800	2.373×10^{-13}	2.386×10^{-14}	2.612×10^{-13}	9.14
900	3.435×10^{-13}	4.457×10^{-14}	3.880×10^{-13}	11.5
1000	4.738×10^{-13}	7.542×10^{-14}	5.492×10^{-13}	13.7
1100	6.298×10^{-13}	1.185×10^{-13}	7.483×10^{-13}	15.8
1200	8.128×10^{-13}	1.757×10^{-13}	9.885×10^{-13}	17.8
1300	1.024×10^{-12}	2.491×10^{-13}	1.273×10^{-12}	19.6
1400	1.264×10^{-12}	3.402×10^{-13}	1.605×10^{-12}	21.2
1500	1.535×10^{-12}	4.509×10^{-13}	1.986×10^{-12}	22.7
1600	1.837×10^{-12}	5.826×10^{-13}	2.420×10^{-12}	24.1
1700	2.172×10^{-12}	7.369×10^{-13}	2.909×10^{-12}	25.3
1800	2.540×10^{-12}	9.152×10^{-13}	3.456×10^{-12}	26.5

[a] K_s refers to the singlet PES, K_t refers to the triplet PES; $K_s + K_t$ stand for the total, single plus triplet, PESs; Γ is the branching ratio (in %) of the triplet PES. The computed tunneling parameters κ are 1.497, 1.198, and 1.023 for K_s at $T = 250$, 298, and 350 K, respectively. For the remaining temperatures and for K_t at all temepratures considered, κ is <1, and therefore, tunneling was not taken into account.

is involved in the alkene ozonolysis processes. The different elementary reaction mechanisms are displayed in Figure 2. Several theoretical studies exist in the literature that covers the unimolecular decomposition of H_2COO.[25−35] However, the different electronic structure of the distinct intermediates along the decomposition path has made the theoretical study of these species difficult. Therefore, we have considered it to be worth extending our investigation to include high-level CASPT2 calculations on these systems.

The geometrical parameters of the corresponding stationary points displayed in Figure 3 were basically reported previously[32,34] and compare quite well with other results from the literature.[31,35] Moreover, in some cases, additional CASSCF geometry optimizations were carried out using either the larger basis set or a larger active space. Further single-point CASPT2 energy calculations were done on the optimized geometries.

Carbonyl oxide (**im1**) can decompose according to two different paths, the fates of which are dioxirane (**im2**) or HCOOH (**im3**). The decomposition path leading to **im3** occurs through **imts3** (see Figures 2 and 3) in a process that involves a H migration from the carbon atom to the terminal oxygen. This process has been already reported by Gutbrod et al.[31] who indicate that **im3** decomposes into HCO + OH with nearly a nonexistent barrier. This is one of the mechanisms that may produce atmospheric formation of OH radicals, and therefore, it is important in tropospheric chemistry. Our computed energy barrier is 35.2 kcal/mol ($\Delta H = 32.5$ kcal/mol), which agrees very well with the best-reported values buy Gutbrod et al.[31]

The **im1** isomerization to dioxirane (**im2**) has been extensively studied in the literature,[26−28,32,35] and the corresponding transition structure is labeled as **imts2** (see Figure 2). It is gratifying to observe that our best computed energy barrier ($\Delta E = 20.1$ kcal/mol and $\Delta H = 18.9$ kcal/mol) and reaction energy ($\Delta E = -28.6$ kcal/mol and $\Delta H = -27.2$ kcal/mol, see also Table 1) are in very good agreement with the high-level CCSD-(T)/(4s3p2d1f/3s2p1d) calculations by Cremer et al.[35] In Table 4, we have also displayed the computed harmonic vibrational frequencies and IR intensities for **im1** and **im2**. Our CASSCF values compare with previous CASSCF reported frequencies[32] and differ from previous CCSD(T) reported values by an average of 110 cm^{-1} for **im1**[29] and 70 cm^{-1} for **im2**[54]. The most intense bands correspond to OO and CO stretching for both structures (see Table 4) in agreement with previous calculated values;[29,32,54] calculated values of the relative intensities have proved to be strongly dependent on the theoretical method used.[29,54]

The following unimolecular decomposition of dioxirane (**im2**) goes on through isomerization to methylenebis(oxy) (**im4**), which may produce formic acid (**im5**), $CO_2 + H_2$ or $CO_2 +$

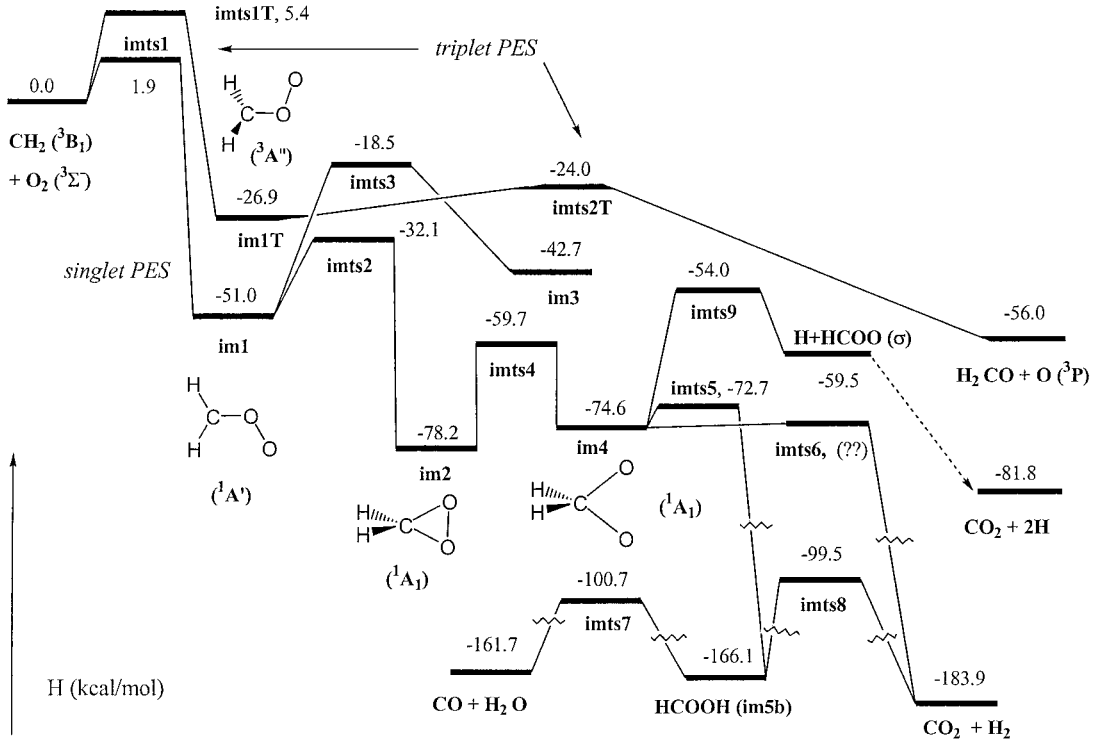

Figure 2. Schematic potential enthalpy diagram showing the relative enthalpies of the whole process considered.

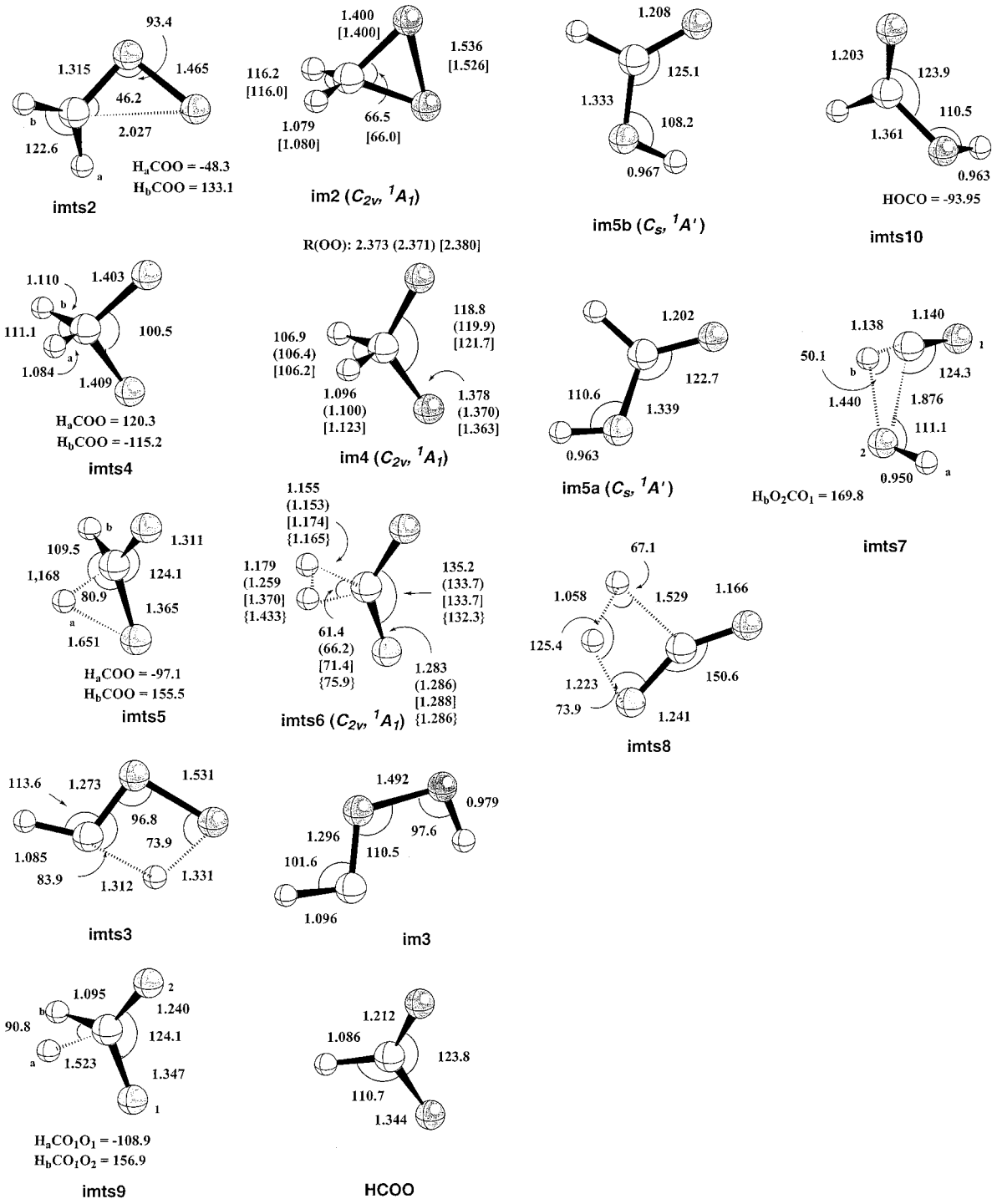

Figure 3. Selected geometrical parameters of the CASSCF stationary points involved in the unimolecular decomposition of H_2COO, X^1A' and A^3A'' electronic states. Values optimized at different levels are designated as follows: single values correspond to CASSCF(8,8)/6-31G(d,p), values in parentheses correspond to CASSCF(12,11)/6-31G(d,p), values in square brackets correspond to CASSCF(18,14)/6-31G(d,p), and values in braces correspond to CASSCF(18,14)/6-311+G(3df,2p).

2H. These reaction modes have been also considered in the literature.[27−30,33,35] However, the carbonyl oxide (**im1**), dioxirane (**im2**), methylenebis(oxy) (**im4**), and the transition structure (**imts6**) of the corresponding symmetric unimolecular dissociation into $H_2 + CO_2$ deserve special interest.

Dioxirane (**im2**) is characterized by the electronic configuration [...$6a_1^2 3b_2^2 2b_1^2 1a_2^2$]; **im1** is mainly described by the electronic configurations [0.94.10a'^{2}1a"^{2}2a"^{2}−0.20.10a'^{2}1a"^{2}-3a"^{2}], while **im4** and **imts6** possess a very strong biradical character. Product **im4** is described mainly by the electronic configurations [0.83...$6a_1^2 3b_2^2 2b_1^2 4b_2^2$−0.50...$6a_1^2 3b_1^2 1a_2^2 4b_2^2$] and **imts6** by [0.89...$6a_1^2 3b_2^2 2b_1^2 4b_2^2$−0.34...$6a_1^2 3b_1^2 1a_2^2 4b_2^2$] (see also ref 33). Please note that b_1, a_2, and a" orbitals are π-type orbitals and the projection of the **im4** and **imts6** configurations into C_s symmetry leads to comparable electronic descriptions for these species to that of **im1**. The distinct electronic description of these species makes it difficult to obtain a balanced description of these electronic structures, and this fact is clearly shown by looking at previous theoretical results from the literature. Thus, for instance, computed relative energy, ΔE(**im4**−**im2**), values of 12.4 kcal/mol (QCISD(T),[28] 11.1 or 8.1 kcal/mol (CASPT2(6,4) or CASPT2(14,12)),[30] 7.1 kcal/mol

TABLE 4: Calculated CASSCF Harmonic Vibrational Frequencies (cm^{-1})[a] and IR Intensities (km mol^{-1}) for im1, im2, and im1T

im1				im2				im1T			
sym	assignment	frequencies	IR int	sym	assignment	frequencies	IR int	sym	assignment	frequencies	IR int
a'	OOC deform	540 (482)	0.7	a_1	OOC deform + OO deform	746 (666)	1.3	a"	CH2 twist	75 (67)	2.4
a"	CH_2 twist	647 (578)	5.9	b_2	CO str asym	931 (831)	21.5	a'	OOC deform	453 (404)	9.8
a'	OO str	867 (774)	301.4	a_2	CH2 twist	1096 (979)	0.0	a'	CH2 wag	799 (713)	14.7
a"	CH_2 wag	903 (806)	34.9	b_1	CH2 rock	1249 (1115)	3.5	a'	OO str	928 (829)	22.9
a'	CO str + CH_2 rock	1271 (1135)	175.7	a_1	CO str sym	1279 (1142)	45.3	a'	CO str	1077 (962)	39.0
a'	CH_2 rock + CO str	1306 (1166)	62.25	b_2	CH2 wag	1367 (1221)	4.1	a"	CH_2 rock	1192 (1064)	6.5
a'	CH_2 scissor	1590 (1420)	31.6	a_1	CH_2 scissor	1671 (1492)	5.3	a'	CH_2 scissor	1563 (1396)	10.6
a'	CH str sym	3297 (2944)	20.9	a_1	CH str sym	3250 (2902)	3.6	a'	CH str sym	3268 (2918)	15.5
a'	CH str asym	3456 (3086)	0.2	b_1	CH str asym	3350 (2991)	5.9	a"	CH str asym	3414 (3048)	7.0

[a] Values in parentheses are scaled by 0.8929 to account for the anharmonic effects.[40]

TABLE 5: Single-Point CASPT2(18,14)/6-311+G(3df,2p) Absolute Energy (in hartree) and Relative Stabilization Energies (values in parentheses, in kcal/mol) for im1, im2, im4, and imts6 Obtained at Different Geometries and Relative Energies (ΔE in kcal/mol) between im1 and im2, im2 and im4, and im4 and imts6

geometry[a]	im1		im2		im4		imts6		ΔE (im1−im2)	ΔE (im2−im4)	ΔE (im4−imts6)
8,8	−189.286 48	(0.00)	−189.331 98	(0.00)	−189.317 95	(0.00)	−189.325 52	(0.00)	−28.55	8.80	−4.80
8,8-c	−189.286 40	(0.05)									
12,11					−189.319 30	(−0.85)	−189.323 62	(1.19)			−2.71
18,14			−189.332 03	(−0.03)	−189.322 11	(−2.61)	−189.322 97	(1.60)		6.22	−0.54
18,14-c							−189.32256	(1.86)			0.63[b]
R	−189.286 67	(−0.12)	−189.332 25	(−0.17)	−189.323 57	(−3.53)			−28.60	5.45	

[a] The designations 8,8; 12,11; and 18,14 stand for the geometry optimized at CASSCF(8,8), CASSCF(12,11), and CASSCF(18,14) with the 6-31G(d,2p) basis set. The designations 8,8-c and 18,14-c stand for the geometry optimized at CASSCF(8,8) and CASSCF(18,14) with the 6-311+G(3df,2p) basis set. R stands for the geometry taken from ref 35, optimized at the MR-AQCC/6-311+G(3df,3pd) level of theory. [b] Relative to the best value of **im4** (−189.323 57 hartree).

(MRD-CI),[33] 5.1 kcal/mol (B3LYP),[35] or 4.6 kcal/mol (MR-AQCC) have been reported.[35] These results indicate differences in the predicted relative energy of these species of up to 7.8 kcal/mol, a value which is about 4 kcal/mol larger than the lowest relative energy predicted. Consequently, we believe that this point merits a more detailed investigation. Because of the impossibility of performing a CASPT2 geometry optimization, we opted, in a first step, to go on combining CASSCF geometry optimizations with single-point CASPT2-(18,14)/6-311+G(3df,2p) energy calculations at the optimized geometries. In a first step, we have limited ourselves by using the 6-31G(d,p) basis set in the CASSCF geometry optimization, but we have enlarged systematically the active space considering up to 18 electrons in 14 orbitals. In a second step and for carbonyl oxide (**im1**), dioxirane (**im2**), and methylenbis(oxy) (**im4**), we have also performed single-point CASPT2(18,14)/6-311+G(3df,2p) calculations on the most reliable geometries from the literature obtained by Cremer et al.[35] by using the MR-AQCC/6-311+G(3df,3pd) theoretical approach. In a third step and for **imts6**, we have also performed a CASSCF-(18,14)/6-311+G(3df,2p) geometry optimization followed by a single-point CASPT2(18,14)/6-311+G(3df,2p) energy calculation. With this series of calculations, we gain dynamical correlation energy in the geometry optimization, which allows us to check its importance in the geometrical parameters and in the relative energies as well. The corresponding results are displayed in Table 5. It shows that for **im1** and **im2** a very small stabilization (0.12 and 0.17 kcal/mol, respectively) is obtained on going from the geometry optimized at CASSCF-(8,8)/6-31G(d,p) to the geometry reported by Cremer et al.[35] However, for **im4**, an important stabilization of 2.61 kcal/mol is obtained on going from the geometry optimized at CASSCF-(8,8)/6-31G(d,p) to the geometry optimized at CASSCF-(18,14)/6-31G(d,p), and this stabilization is enlarged to 3.53 kcal/mol if we consider the best geometry reported by Cremer et al.[35] In a similar way, **imts6** is destabilized up to 1.6 kcal/mol on going from the geometry optimized at CASSCF(8,8)/6-31G(d,p) to the geometry optimized at CASSCF(18,14)/6-31G(d,p) or up to 1.86 kcal/mol when the optimized geometry was obtained at the CASSCF(18,14)/6-311+G(3df,2p) level. The interest of these results is clearly reflected by the ΔE relative energies displayed also in Table 5. Thus, taking the geometries optimized at CASSCF(8,8)/6-31G(d,p), we obtain a ΔE(**im2**−**im4**) of 8.8 kcal/mol and the transition state **imts6** is computed to be lower in energy than the corresponding minima **im4** (ΔE(**im4**−**imts6**) = −4.8 kcal/mol). However, considering the best geometry that we have available to perform the CASPT2 single-point calculations (see Table 5), we calculated a ΔE(**im2**−**im4**) of 5.45 kcal/mol in very good agreement with the result reported by Cremer et al.[35] and ΔE(**im4**−**imts6**) = 0.63 kcal/mol. On the other side, no appreciable changes are observed for ΔE(**im1**−**im2**) obtained with the CASSCF or the best MR-AQCC geometries. These results point out the importance of the dynamical correlation energy for the **im4** and **imts6** species,

which possess a very strong biradical character, not only for obtaining good estimates of the relative energies but also for obtaining a good prediction of the optimized geometries. Please also note from Tables 4 and 1 that even considering the best treatments at the MR-AQCC geometry reported by Cremer et al.[35] for **im2** and CASSCF(18,14)/6-311+G(3df,2p) for **imts6**, the corresponding energy barrier is still negative when considering the ZPE or the enthalpy corrections. This fact indicates that we still do not have an optimum geometry for the transition state, provided that the minima were optimized with a method that considers explicitly the dynamic correlation energy. These energy data and the corresponding geometrical parameters displayed in Figure 3, especially for **im4** and **imts6**, make also evident the well-known fact that CASSCF exaggerates the bond lengths.

Regarding the two additional decomposition modes of methylenebis(oxy) (**im4**), the first one is labeled as **imts5** (Figure 2) and produces *syn*-formic acid (**im5b**). The computed energy barrier is very low ($\Delta E = 3.8$ kcal/mol or $\Delta H = 1.9$ kcal/mol), and the highly exothermic reaction energy ($\Delta H = -91.5$ kcal/mol) compares quite well with other values from the literature.[34,35] The second one, which is labeled as **imts9**, involves the homolytic cleavage of one CH bond forming H + HCOO. Here, we report an energy barrier of 24.9 kcal/mol ($\Delta H = 20.6$ kcal/mol), a value that is about 3 kcal/mol larger than those reported previously[34] and that reflects the best description of **im4** obtained in the present work. HCOO was also reported to decompose into H + CO_2 with a very small energy barrier.[34]

Finally, the computed unimolecular decomposition of formic acid (**im5a** and **im5b**, which isomerizes through **imts10**) into $CO_2 + H_2$ (through **imts8**, $\Delta E = 68.3$ kcal/mol and $\Delta H = 62.1$ kcal/mol) and into $CO + H_2O$ (through **imts7**, $\Delta E = 69.8$ kcal/mol and $\Delta H = 65.4$ kcal/mol) (see also Table 1 and Figure 2) compares also well with previous results from the literature.[34,35]

Unimolecular Decomposition of the Triplet Carbonyl Oxide (H_2COO, A^3A''): The Formation of $H_2CO + O(^3P)$. This reaction proceeds by an elongation of the OO bond in **im1T** leading to the formation of formaldehyde (H_2CO) and atomic oxygen (^3P) (see **imts2T** in Figure 2). This process has been already reported in the literature,[32] and here, we aimed only to provide better activation and reaction energies obtained using a much better basis set than previously. Our computed energy barrier of 4.1 kcal/mol ($\Delta H = 2.9$ kcal/mol) compares very well with the previous value reported in the literature.[32] This reaction is computed to be exothermic by 29.1 kcal/mol, which also compares with the results from the literature.[32] At this point it is also worth reminding the reader that, besides the unimolecular decomposition of **im1T**, the triplet PES crosses the singlet PES in a geometry close to **im1T**. However, calculations of the spin−orbit coupling matrix indicated that this intersystem crossing (ISC) should be inefficient. [32]

Conclusions

In this work, we have investigated the reaction between CH_2 (X^3B_1) and O_2 ($X^3\Sigma^-$) by means of CASSCF and CASPT2 quantum chemistry calculations. The following points come out from the present investigation.

(1) The reaction between CH_2 (X^3B_1) and O_2 ($X^3\Sigma_g^-$) may follow both a singlet and a triplet potential energy surface. The singlet PES leads to the formation of carbonyl oxide H_2COO, (**im1**, X^1A', C_s) in a process that is computed to be exothermic by about 52 kcal/mol and for which we have calculated an enthalpy barrier of about 2 kcal/mol. The triplet PES follows throughout an enthalpy barrier of 5.4 kcal/mol and produces also carbonyl oxide in its triplet excited state (**im1T**, A^3A'', C_s). This process is computed to be exothermic by about 32 kcal/mol.

(2) We have computed the rate constants for both the singlet and triplet PES, in the 250−1800 K range, applying the classical transition-state theory, which allow us to estimate the corresponding branching ratio (Γ). The computed rate constants are about 300 times smaller than the estimated experimental values. However, despite these differences, we believe that we calculate accurate Γ values because both the singlet and triplet PESs are computed at the same level of accuracy. Thus, we have estimated the branching ratio for the triplet PES (which leads to the formation of O (^3P) atom) to be negligible at 250 K but to rise up to 26% at 1800 K.

(3) We have also considered the unimolecular decomposition of carbonyl oxide (**im1**) (X^1A') and the obtained results compare quite well with previous results reported in the literature.[34,35] Compound **im1** can either isomerize to HCOOH (**im3**), which dissociates into HCO + OH with an activation enthalpy of 32.5 kcal/mol, or isomerize to dioxirane (**im2**) requiring an activation enthalpy of 18.7 kcal/mol. The subsequent decomposition goes on through isomerization to methylenebis(oxy) (**im4**), which may decompose producing $CO_2 + H_2$, HCOOH, and H + HCO. Carbonyl oxide (**im1**), dioxirane (**im2**), methylene(bis)oxy (**im4**), and **imts6** have deserved special interest. The very strong biradical character of **im4** and **imts6** leads to a strong dependence on the theoretical method used to obtain accurate results. Our calculations indicate the need to use methods that include dynamical correlation energy for both the optimized geometry and the relative energy to obtain accurate results for these species. For the remaining structures, which do not possess as strong a biradical character, our results, which compare with others from the literature,[35] indicate that large scale CASPT2 calculations carried out over CASSCF optimized geometries provide good results.

4) The triplet H_2COO (**im1T**) (A^3A'') decomposes into H_2CO (X^1A_1) + O (^3P_g). The process is computed to be exoergic by about 27 kcal/mol and has an activation enthalpy of 2.9 kcal/mol.

Acknowledgment. The financial support to this work was provided by China National Natural Science Foundation with the Contracts 29892160 and 29773052 and by the Dirección General de Investigación Científica y Técnica (DGICYT, Grant PB98-1240-C02-02) in Spain. The calculations described in this work were performed at Beijing and at the Centre de Supercomputació de Catalunya (CESCA), the SGI Power Challenge and at the HP 7200 of the IIQAB-CSIC in Barcelona. We also thank Prof. S. D. Peyerimhoff and Dr. M. W. Schmidt for providing a copy of the MRD-CI and GAMESS codes, respectively.

Supporting Information Available: Active space composition of all stationary points and Cartesian coordinates and absolute energies of all structures. This material is available free of charge via the Internet at http://pubs.acs.org.

References and Notes

(1) Laufer, A. H. *Rev. Chem. Intermed.* **1981**, *4*, 225.
(2) Miller, J. A.; Kee, R. J.; Westbrook, C. K. *Annu. Rev. Phys. Chem.* **1990**, *41*, 345.
(3) Alvarez, R. A.; Moore, C. B. *J. Phys. Chem.* **1994**, *98*, 174.
(4) Bley, U.; Temps, F. Wagner, H. Gg.; Wolf, M. *Ber. Bunsen-Ges. Phys. Chem.* **1992**, *96*, 1043.
(5) Dombrowsky, Ch.; Hwang, S. M.; Rohrig, M.; Wagner, H. Gg. *Ber. Bunsen-Ges. Phys. Chem.* **1992**, *96*, 194.

(6) Dombrowsky, C.; Wagner, H. Gg. *Ber. Bunsen-Ges. Phys. Chem.* **1992**, *96*, 1048.
(7) Hsu, D. S. Y.; Lin, M. C. *Int. J. Chem. Kinet.* **1997**, *9*, 507.
(8) Shaub, W. M.; Hsu, D. S. Y.; Burfs, T. L.; Lin, M. C. *Symp. (Int). Combust., [Proc.], 18th* **1981**, 811.
(9) Su, H.; Mao, W.; Kong, F. *Chem. Phys. Lett.* **2000**, *321*, 89.
(10) Strachan, A. N.; Noyes, W. A. *J. Am. Chem. Soc.* **1954**, *76*, 3258.
(11) Holroyd, R. A.; Noyes, W. A. *J. Am. Chem. Soc.* **1956**, *78*, 4831.
(12) Rusell, R. L.; Rowland, F. S. *J. Am. Chem. Soc.*, **1968**, *90*, 1671.
(13) Hatakeyama, S.; Bandow, H.; Okuda, M.; Akimoto, H. *J. Phys. Chem.* **1981**, *85*, 2249.
(14) Laufer, A. H.; Bass, A. M. *J. Phys. Chem.* **1974**, *78*, 1344.
(15) Pilling, M. J.; Robertson, J. A. *J. Chem. Soc., Faraday Trans.* **1977**, *73*, 968.
(16) Vinckler, C.; Debruyn, W. *J. Phys. Chem.* **1979**, *83*, 2057.
(17) Baulch *J. Phys. Chem. Ref. Data* **1992**, *21* (3), 639.
(18) Su, F.; Calvert, G.; Shaw, J. H. *J. Phys. Chem.* **1980**, *84*, 239.
(19) Kan, C. S.; Su, F.; Calvert, G.; Shaw, J. H. *J. Phys. Chem.* **1981**, *85*, 2363.
(20) Martinez, R. I.; Herron, J. T. *J. Phys. Chem.* **1987**, *91*, 946.
(21) Neeb, P.; Horie, O.; Moortgat, G. K. *J. Phys. Chem. A* **1998**, *102*, 6778.
(22) Mihelcic, D.; Heitlinger, M.; Kley, D.; Müsgen, P.; Volz-Thomas, A. *Chem. Phys. Lett.* **1999**, *301*, 559.
(23) Paulson, S. E.; Chung, M. Y.; Hasson, A. S. *J. Phys. Chem. A* **1999**, *103*, 8127.
(24) Kroll, J. H.; Clarke, J. S.; Donahue, N. M.; Anderson, J. G.; Demerjian, K. L. *J. Phys. Chem. A* **2001**, *105*, 1554.
(25) Wadt, W. R.; Goddard, W. A., III *J. Am. Chem. Soc.* **1975**, *97*, 3004.
(26) Karlström, G.; Roos, B. O. *Chem. Phys. Lett.* **1981**, *79*, 416.
(27) Cimiraglia, R.; Ha, T. K.; Meyer, R.; Cünthard, H. H. *Chem. Phys.* **1982**, *66*, 209.
(28) Bach, R. D.; Andres, J. L.; Owensby, A. L.; Schlegel, H. B.; McDouall, J. J. W. *J. Am. Chem. Soc.* **1992**, *114*, 7207.
(29) Cremer, D.; Gauss, J.; Kraka, E.; Stanton, J. F.; Bartlett, R. J. *Chem. Phys. Lett.* **1993**, *209*, 547.
(30) Cantos, M. Merchán, M.; Tomás-Vert, F.; Roos, B. O. *Chem. Phys. Lett.* **1994**, *229*, 181.
(31) Gutbrod, R.; Schindler, R. N.; Kraka, E.; Cremer, D. *Chem. Phys. Lett.* **1996**, *252*, 221.
(32) Anglada, J. M.; Bofill, J. M.; Olivella, S.; Sole, A. *J. Am. Chem. Soc.* **1996,** *118*, 4636.
(33) Anglada, J. M.; Bofill, J. M.; Olivella, S.; Sole A. *J. Phys. Chem. A* **1998**, *102*, 3398.
(34) Anglada, J. M.; Crehuet, R.; Bofill, J. M. *Chem.—Eur. J.* **1999**, *5*, 1809.
(35) Cremer, D.; Kraka, E.; Szalay, P. G. *Chem. Phys. Lett.* **1998**, *292*, 97.
(36) Roos, B. O. *Adv. Chem. Phys.* **1987**, *69*, 399.
(37) Baker, J. *J. Comput. Chem.* **1986**, *7*, 385.
(38) Baker, J. *J. Comput. Chem.* **1987**, *8*, 563.
(39) Bofill, J. M *J. Comput. Chem.* **1994**, *15*, 1.
(40) Curtiss, L. A.; Raghavachari, K.; Trucks, G. W.; Pople, J. A. *J. Chem. Phys.* **1991**, *94*, 7221.
(41) Anglada, J. M.; Bofill, J. M. *Chem. Phys. Lett.* **1995**, *243*, 151.
(42) Buenker, R. J.; Peyerimhoff, S. D. *Theor. Chim. Acta* **1975**, *39*, 217.
(43) Buenker, R. J.; Peyerimhoff, S. D. In *New Horizons of Quantum Chemistry*; Lowdin, P. O., Pullman, B., Eds.; D. Reidel: Dordrecht, The Netherlands, 1983; Vol. 35, p 183.
(44) Buenker, R. J.; Philips, A. *THEOCHEM* **1985**, *123*, 291.
(45) Hariharan, P. C.; Pople, J. A. *Theor. Chim. Acta* **1973**, *28*, 213.
(46) (a) Krishnan, R.; Binkley, J. S.; Seeger, R.; Pople, J. A. *J. Chem. Phys.* **1980**, *72*, 650. (b) Clark, T.; Chandrasekhar, J.; Spitznagel, G. W.; Sheleyer, P. v. R. *J. Comput. Chem.* **1983**, *4*, 294. (c) Frish, M. J.; Pople, J. A.; Binkley, J. S. *J. Chem. Phys.* **1984**, *80*, 3265.
(47) Andersson, K.; Roos, B. O. *Int. J. Quantum Chem.* **1993**, *45*, 591.
(48) Andersson, K.; Malmqvist, P.; Roos, B. O. *Modern Electronic Structure Theory*; Yarkony, D. R., Ed.; World Scientific: Signapore, 1995; Part 1, p 55.
(49) Frisch, M. J.; Trucks, G. W.; Schlegel, H. B.; Scuseria, G. E.; Robb, M. A.; Cheeseman, J. R.; Zakrzewski, V. G.; Montgomery, J. A., Jr.; Stratmann, R. E.; Burant, J. C.; Dapprich, S.; Millam, J. M.; Daniels, A. D.; Kudin, K. N.; Strain, M. C.; Farkas, O.; Tomasi, J.; Barone, V.; Cossi, M.; Cammi, R.; Mennucci, B.; Pomelli, C.; Adamo, C.; Clifford, S.; Ochterski, J.; Petersson, G. A.; Ayala, P. Y.; Cui, Q.; Morokuma, K.; Malick, D. K.; Rabuck, A. D.; Raghavachari, K.; Foresman, J. B.; Cioslowski, J.; Ortiz, J. V.; Stefanov, B. B.; Liu, G.; Liashenko, A.; Piskorz, P.; Komaromi, I.; Gomperts, R.; Martin, R. L.; Fox, D. J.; Keith, T.; Al-Laham, M. A.; Peng, C. Y.; Nanayakkara, A.; Gonzalez, C.; Challacombe, M.; Gill, P. M. W.; Johnson, B. G.; Chen, W.; Wong, M. W.; Andres, J. L.; Head-Gordon, M.; Replogle, E. S.; Pople, J. A. *Gaussian 98*, revision A.6; Gaussian, Inc.: Pittsburgh, PA, 1998. Frisch, M. J.; Trucks, G. W.; Schlegel, H. B.; Gill, P. M. W.; Johnson, B. G.; Robb, M. A.; Cheeseman, J. R.; Keith, T.; Petersson, G. A.; Montgomery, J. A.; Raghavachari, K.; Al-Laham, M. A.; Zakrzewski, V. G.; Ortiz, J. V.; Foresman, J. B.; Cioslowski, J.; Stefanov, B. B.; Nanayakkara, A.; Challacombe, M.; Peng, C. Y.; Ayala, P. Y.; Chen, W.; Wong, M. W.; Andres, J. L.; Replogle, E. S.; Gomperts, R.; Martin, R. L.; Fox, D. J.; Binkley, J. S.; Defrees, D. J.; Baker, J.; Stewart, J. P.; Head-Gordon, M.; Gonzalez, C.; Pople, J. A. *Gaussian 94*, revision E.1; Gaussian, Inc.: Pittsburgh, PA, 1995.
(50) Schmidt, M. W.; Baldrige, K. K.; Boatz, J. A.; Jensen, J. H.; Koseki, S.; Gordon, M. S.; Nguyen, K. A.; Windus, T. L.; Elbert, S. T. *QCPE Bull.* 1990, *10*, 52.
(51) Andersson, K.; Blomberg, M. R. A.; Fülscher, M. P.; Karlstrom, G.; Lindh, R.; Malmqvist, P.; Neogrady, P.; Olsen, J.; Roos, B. O.; Sadlej, A. J.; Schutz, M.; Seijo, L.; Serrano-Andres, L.; Siegbahn, P. E. M.; Widmark, P. O. *MOLCAS*, version 4.1; Lund University: Lund, Sweden, 1998.
(52) Truong, T. N.; Truhlar, D. G. *Chem. Phys.* **1990**, *93*, 1761.
(53) Duncan, W. T.; Truong, T. N. http://therate.hec.utah.edu (accessed September 2000).
(54) Kim, S. J.; Schaefer, H. F., III; Kraka, E.; Cremer, D. *Mol. Phys.* **1996**, *88*, 93.